Mechanical-Chemical Activation of Coal Fly Ashes: An Effective Way for Recycling and Make Cementitious Materials

Ana Fernández-Jiménez, Ines Garcia-Lodeiro*, Olga Maltseva and Angel Palomo

Department of Materials, Eduardo Torroja Institute, Consejo Superior de Investigaciones Científicas (CSIC), Madrid, Spain

This paper is wholly committed to resource efficiency through the valorization of waste from other industries, and more specifically fly ash as a raw material to produce concrete-like geopolymers. In particular, this study aimed to determine the effect of the physical and chemical characteristics of recycled coal fly ash used to manufacture alkaline cement on reaction kinetics and product microstructure and performance. The ash was mixed with 8 M NaOH and cured for 20 h at 85°C and RH > 90% to form a compact paste, after which mechanical strength was determined and the reaction rate was calculated using isothermal conduction calorimetry. The findings showed that vitreous content (SiO_2/Al_2O_3), reactive and (especially) fineness play a very important role in both the development of cement mechanical strength and the composition and structure of the reaction products formed.

Keywords: recycling, fly ash, alkaline activation, geopolymer, mechanical-chemical activation, NMR

INTRODUCTION

Portland cement manufacture consumes around 4 GJ of energy per ton and accounts for approximately 8% of worldwide CO_2 emissions, or 2.981 $GtCO_{2eq}$ in 2014 (CSI/ECRA—Cement Sustainability Initiative/ European Cement Research., 2017).

The Roadmap for a resource-efficient Europe (COM, 2011) 0571 describes industrial strategies to mitigate the effects of industrial activity and ensure that by 2050 Europe will have a sustainable economy, in which "resources are not simply extracted, used and thrown away, but are put back in the loop so they can stay in use for longer."

Cross-cutting concerns such as the need for more long-term, innovative thinking are also being addressed. The research supporting this paper is wholly committed to resource efficiency through the valorization of waste from other industries, and more specifically, fly ash as a raw material to produce concrete-like "geopolymers," which contain a drastically reduced proportion of portland cement.

Worldwide production of combustion products (CCPs), including fly ash, amounted to 780 Mt in 2011 and nearly 1 Gt in 2015. Whilst the rate of re-use varies widely from country to country (10.6–96.4%), overall 47% of the fly ash generated is presently landfilled (Thomas, 2007). Options for reusing CCPs, which have been under study around the world for the last 70 years, can be classified as non-beneficial, simply transformed manufactures (STM) or elaborately transformed manufactures (ETM). Like other industrial waste such as blast furnace slag or red mud, fly ash can be activated in alkaline media, setting and hardening to acquire properties similar to

those characteristics of portland cement. Such materials, known as "alkali-activated cements" or "geopolymers," constitute optimal vehicles for valorizing and recycling coal fly ash (Palomo et al., 2014; Zhuang et al., 2016; Bai and Colombo, 2018).

The 500 Mt/year of coal fly ash presently landfilled could be reused to manufacture cement or concrete (Chindaprasirt et al., 2005; Duvallet et al., 2015; Hemalatha and Ramaswamy, 2017) if ash particle reactivity could be significantly enhanced. Such valorization would also help mitigate global warming by reducing the CO_2 emitted by the building materials industry. The primary objective of the present study was consequently to devise processing methods that would heighten fly ash reactivity.

The main reaction product formed in the alkali activation of fly ash is an amorphous, three-dimensional alkaline inorganic polymer generically known as N-A-S-H (Na_2O-Al_2O_3-SiO_2-H_2O) gel (Fernández-Jiménez et al., 2005; Provis and van Deventer, 2014). Secondary reaction products may include zeolites such as Na-chabazite, zeolites A and P, and faujasite (Fernández-Jiménez et al., 2005; Panias et al., 2007).

Earlier studies have shown an intrinsic relationship between the composition and structure of N-A-S-H gel and its physical and mechanical properties (Fernández-Jiménez et al., 2006; De Silva et al., 2007). Given similar degrees of reaction, the formation of N-A-S-H gels with an Si/Al ratio of ≈1 (type 1 gels) yields materials with lower mechanical strength than when the gel formed has an Si/Al ratio of ≈2 (type 2 gels) (Fernández-Jiménez et al., 2006; Hajimohammadi et al., 2010; Nikolic et al., 2015). Further studies by a number of authors (Sagoe-Crentsil et al., 2005; Kovalchuk et al., 2007; Fernández-Jiménez et al., 2017) optimal Si/Al ranges from 2 to 4. Such findings attest to the importance of the reactive silica and alumina content in the starting materials, which largely conditions the ultimate composition of the gel formed. In high calcium based systems (such as type C fly ashes), the initial setting process is governed by the formation of C-S-H or C-A-S-H-like phases rather than pure N-A-S-H. Fast dissolution of highly active Al_2O_3 and SiO_2 sources in high pH medium provides high initial concentrations of silicate species and aluminate to react with Ca forming C-A-S-H phase in the early reaction stages (Chindaprasirt et al., 2012). Other works developed in the field of hybrid alkaline cements (systems with small OPC contents + high content of an aluminosilicate source) point out the co-precipitation of both C-A-S-H+ (N,C)-A-S-H gels during the early reaction stages, which would evolve with time to a C-A-S-H gel (Garcia-Lodeiro et al., 2011, 2013).

In addition to the chemical composition of the ash, the vitreous phase content and the $(SiO_2/Al_2O_3)_{reactive}$ ratio, particle size is a factor to be borne in mind when determining a material's reactive potential. A number of studies mention the effect of fly ash particle size when used either as a supplementary cementitious material to lower the clinker factor (Paya et al., 1997; Chindaprasirt et al., 2005; Hemalatha and Ramaswamy, 2017) or as a precursor in the preparation of alkaline (OPC-less) cements (Fernández-Jiménez et al., 2005; Marjanovic et al., 2014; Duvallet et al., 2015).

Many authors (Rakesh et al., 2007; Temuujin et al., 2009; Kumar and Kumar, 2011; Kumar et al., 2015; Shekhovtsova

et al., 2018) have broached the effect of fineness on ash reactivity, separating the material either by sieving (particles under 45 μm (Duvallet et al., 2015) or electrostatic precipitation (Kumar et al., 2015). Their findings have consistently shown that mechanical strength rises substantially with ash fractions of under 45 μm. Particle size separation normally prompts an increase in the proportion of vitreous phase, for the particles eliminated (the largest) consist essentially in scantly reactive crystalline phases such as quartz, unburnt carbon, and hematite. The discards generated by such processes would, naturally, need to be managed.

Kumar et al. have published a host of papers on the mechanical activation of fly ash (Kumar and Kumar, 2011; Kumar et al., 2015). They observed that milling fly ash raised the mechanical strength of the resulting cements, which they attributed both to the stimulation of ash reactivity by the smaller particle size (particularly at early ages) and to physical changes in porosity and the pore size distribution of the end product. Temuujin et al. (2009), however, observed no clear correlation between the rise in strength and changes in material porosity and density. The general consensus in the literature to date (Kumar and Kumar, 2011; Kumar et al., 2015) is that the mechanical activation of fly ash enhances the mechanical strength of the end product because the changes in particle morphology along with size hasten dissolution-precipitation reactions, raising reactivity. That in turn yields more compact microstructures, with a larger amount of gel and smaller fraction of unreacted particle (Zhang et al., 2016).

Most papers published on the effect of the mechanical activation of ash focus on a single material, with very few comparing the effect in ash from different sources (Marjanovic et al., 2014; Kumar et al., 2015). In a recent article proposing an equation to assess the suitability of fly ash for the production of a high-strength geopolymer, Zhang et al. (2016) reported that physical properties (density, specific surface, and fineness) may have a greater effect on ash reactivity than its vitreous phase content.

In light of the foregoing, the present study aimed to determine the effect of the mechanical activation of ash (by milling) on strength development, reaction kinetics and micro- and nanostructure of the reaction products.

The materials used had different vitreous phase contents and $(SiO_2/Al_2O_3)_{reactive}$ fractions. Their initial particle size also differed, although they were ground for a sufficient time to substantially modify the specific surface of the original ash. The three ashes were ground and alkali-activated, after which their mechanical strength was determined and the reaction products were characterized by using XRD, SEM/EDX, and NMR.

EXPERIMENTAL

Materials

The three fly ashes used in this study, sourced from different Chinese steam plants, had different chemical and mineralogical compositions. Their chemical composition (% of oxides by mass), found with a PHILIPS PW 2400 X-ray fluorescence spectrometer fitted with a PW 2540 VTC sample changer, is given in **Table 1**.

TABLE 1 | Bulk chemical composition of the coal fly ash studied.

	F1	F2	F3
SiO_2	58.02	45.18	42.68
Al_2O_3	18.7	33.59	49.36
CaO	9.82	9.36	2.21
Fe_2O_3	4.10	4.54	1.45
K_2O	3.10	1.13	0.32
Na_2O	1.59	1.07	–
MgO	1.36	0.83	–
SO_3	0.50	0.74	0.12
TiO_2	0.79	1.26	1.67
CrO	0.13	0.18	0.07
MnO	0.11	0.11	/
Other	1.03	0.29	0.26
Lol	0.79	1.72	1.86
Total	100	100	100
SiO_2/Al_2O_3	3.10	1.34	0.86
Minor crystalline phases	Quartz caO	Quartz corundum mullite caO	Corundum mullite

The table also shows the XRD-detected minority crystalline phases in each ash. The significant differences in aluminum content prompted a fairly wide-ranging initial SiO_2/Al_2O_3 ratio, from 3.10 to 0.86.

Experimental

Particle size distribution was determined on a COULTER LS 130 laser sizer with a measuring range of 0.1–900 μm. The ash was ground in a laboratory ball grinder for 4 h (regarded as sufficient time to ensure similar particle size distributions in all three varieties of ash), using the same number of balls and loading the grinder with the same weight of sample throughout.

The materials were exposed to an acid attack (continuously stirring 1 g of ash in 100.00 mL of a 1% HF solution for 5 h (Ruiz-Santaquiteria et al., 2013) to quantify the potential reactivity of both the unground original (F1, F2, and F3) and ground (GF1, GF2 and GF3) ash. The resulting solution was then filtered, the residue was rinsed with distilled water to a neutral pH and the amount of dissolved (=potentially reactive) silica and alumina in the leachate was quantified by ICP on a Varian 725-ES optical ICP atomic emission spectrometer with the following settings: power, 1.40 kW; plasma gas flow, 15.00 L/min; nebulizer gas flow, 0.85 L/min; read time, 5 s. The findings were used to calculate the $(SiO_2/Al_2O_3)_{reactive}$ ratio for each ash.

The ground and unground ashes were mixed with an 8 M NaOH solution and the resulting pastes molded into prismatic specimens measuring $1 \times 1 \times 6$ cm^3 to determine whether these materials were susceptible to alkali activation and able to yield a product with good mechanical properties. The alkaline solution/ash ratio varied depending on the ash (see **Table 2**), yet was the same for the ground and unground versions of each. The samples were cured for 20 h in an oven at 85°C and a relative humidity of ≥90%. These conditions usually guarantee a proper

TABLE 2 | Mechanical strength of alkali-activated paste prepared with ground or unground coal fly ash and cured for 20 h at 85°C.

Fly ash	8 M NaOH /FA ratio (wt)	Compressive strength (MPa) in 1 day pastes		Δ Strength (est., %)
		Original	Ground	
F1Na	0.35	17.04 ± 0.96	29.26 ± 2.17	41.8
F2Na	0.35	27.29 ± 1.74	46.39 ± 2.63	41.2
F3Na	0.4	1.33 ± 0.20	18.13 ± 1.82	92.66

FA reactivity (Fernández-Jiménez and Palomo, 2007; Zhou et al., 2016). The compressive strength of the specimens was found on an Ibertest Autotest 200/10-SW frame 24 h after mixing. Ten specimens of each composition were tested.

The starting ashes and reaction products were characterized by XRD, scanning electron microscopy (SEM/EDX) and NMR. X-ray diffraction (XRD) was conducted on a Bruker AXS D8 ADVANCE diffractometer. The scanning spectrum ranged from 2Θ angles 5 to 60° with a nominal step size of 0.0119736° at a rate of 0.5 s/step. Powder samples were exposed to Cu-Kα1, α2 X-ray radiation.

Fly ash morphology and cured specimen microstructure were examined under a JEOL 5400 scanning electron microscope fitted with an OXFORD LINK-ISIS EDX (energy dispersive X-ray) system. EDS analyses (on spots) were done with accelerating voltage of 20 kV, working distance of 15 mm and beam current of 20 μA and acquiring for 60 s per spot analysis. An average of 50 analys were taken per sample.

The NMR scans were recorded on a BRUKER AVANCE-400 spectrometer. All the samples were spun at 10 kHz. For ^{27}Al MAS-NMR, the settings were: frequency, 104.3 MHz; 2 ms single pulse MAS; 5 s relaxation delay; external standard, $Al(H_2O)_6$. For ^{23}Na MAS-NMR they were: frequency, 105.8 MHz; 2 ms single pulse MAS; 5 s relaxation delay; external standard, NaCl. For ^{29}Si MAS-NMR the data were: frequency 79.5 MHz; 5 ms single pulse MAS; 10 s relaxation delay; external standard, TMS.

Ash reaction rate was determined in terms of heat flow calculated using isothermal conduction calorimetry. Pastes were prepared by adding 5 g of fly ash to 2.5 g of alkaline solution to ensure satisfactory mixing. The paste was mixed manually for 3 min *ex-situ* in a sample cell, which was subsequently sealed and then immediately placed in a TAM Air Thermometric calorimeter where heat flow was recorded at a constant external temperature of 85 ± 1°C.

RESULTS AND DISCUSSION

Effect of Grinding on Ash Physical and Chemical Characteristics

Figure 1 shows the particle size distribution of the fly ash as received from the steam-fired power plants and after grinding. Ash F1 initially had a median particle size, d_{50}, of 9 μm; ash F2 of around 20 μm; and F3, the coarsest, a value of approximately 34 μm. After grinding, these differences narrowed substantially, with all three types of ash exhibiting d_{50} values of 5 μm to 7 μm.
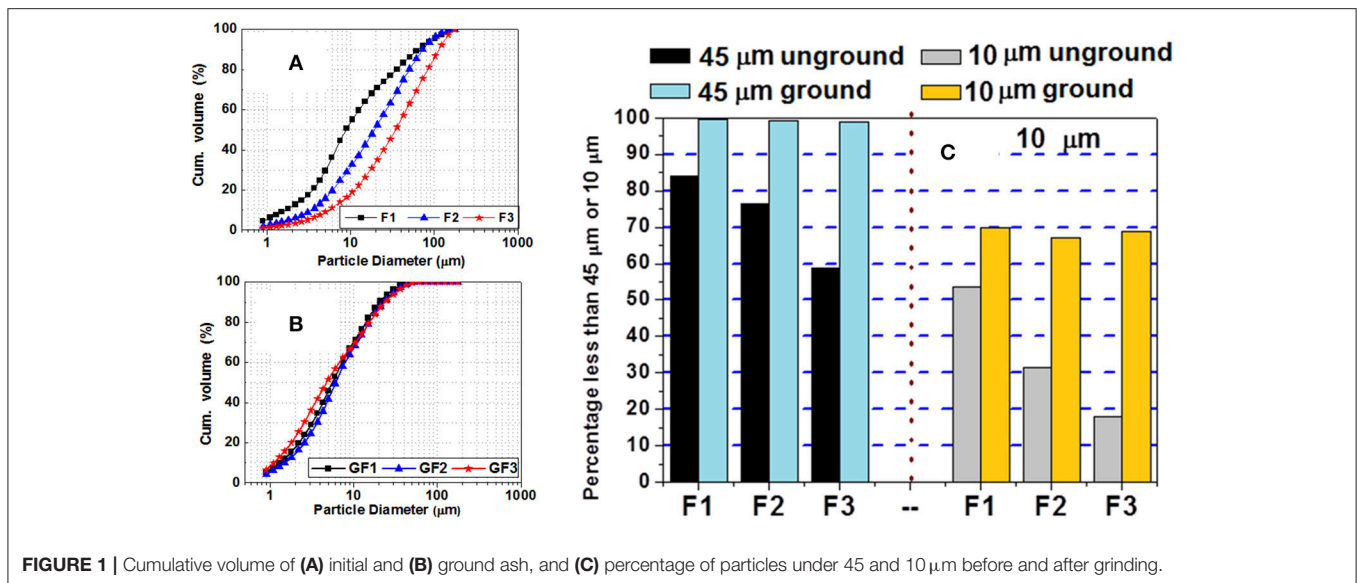
FIGURE 1 | Cumulative volume of **(A)** initial and **(B)** ground ash, and **(C)** percentage of particles under 45 and 10 μm before and after grinding.

The effect of grinding is graphically illustrated in **Figure 1C**, which shows the percentage of particles under 45 and 10 μm before and after milling. Grinding clearly yielded a more uniform particle size in all three varieties of ash, with 98% of the particles under 45 and 67% under 10 μm. The most significant change was observed in F3, the ash with the initially largest particle size. The data in **Figure 1** show that ashes with initially different particle sizes exhibited fairly similar distributions after grinding. The inference appears to be that below a given threshold particle size, the grinding system used was ineffective.

Based on their chemical composition (**Table 1**: $SiO_2 + Al_2O_3 + Fe_2O_3 \geq 70\%$; $CaO < 10\%$), F1, F2, and F3 constituted what is regarded by European standard EN 450-1 and ASTM standard C 618 as class F fly ash, i.e., pozzolanic ash resulting from the combustion of anthracite or bituminous coal. Further, to Canadian standard CSA A3001, however, which classifies fly ash in three groups depending on CaO content, only ash F3 would qualify as class F: silicoaluminous, low calcium fly ash with <8% CaO, consisting predominantly in aluminosilicate glass with varying amounts of crystalline quartz, mullite, hematite and magnetite. In the Canadian system, both F1 and F2 would be class C1 (8–20% CaO) ash, with an intermediate proportion of calcium oxide.

The results of the acid attack conducted to determine ash reactivity are compared in **Figure 2** to the overall silica and alumina contents found with chemical analysis. As the sum of the reactive silica and alumina was not over 70% in any of the materials studied, all three could be defined as Canadian standard class C1 ash.

Figure 2 shows that grinding-based mechanical activation barely modified the potentially reactive silica and alumina identified in the starting ash. In other words, particle size would not initially appear to have any significant effect on the reactive potential of the ash. The figure also reveals the clearly smaller reactive than bulk aluminum content in ground and unground

ashes F2 and F3. In these two materials, bulk alumina was on the order of 30–50% whilst the potentially reactive compound accounted for no more than 10%.

The SEM micrographs (see **Figure S1**) showed that the ashes with coarser particle sizes (F2 and F3) prior to grinding exhibited a more heterogeneous morphology, whereas the finer ash (F1) was more uniform and had a higher proportion of spherical particles.

The diffractograms for the original ash contained a hump at 2Θ values of 20–35° associated with the vitreous content of the ash. The intensity of this hump is usually related to the amorphous content. The minority crystalline phases identified were quartz, mullite, hematite, corundum and traces of CaO. The corundum and mullite contents were high in ashes F2 and F3, which justify the lower intensity of the hump in these two with respect to F1. No significant mineral differences were observed between the pre-and post-ground ash diffractograms. The sole visible changes included a slight decline in the intensity of the quartz diffraction line, which might explain the slight increase in the soluble SiO_2 content in the ground ash (see **Figure 2**), and a rise in the diffraction line for hematite, possibly attributable to the use of iron grinding balls.

The ^{27}Al NMR spectra (see **Figure 3**) for the original ash contained an aluminum signal at around 58 to 60 ppm associated with tetrahedral aluminum (Al_T), present primarily in the vitreous phases of fly ash. Ash F1 clearly contained no octahedral aluminum (Al_O), a finding consistent with the HF chemical attack results (see **Figure 2**), according to which nearly all the alumina present in this ash was reactive. In varieties, F2 and F3 mullite were detected as a shoulder at ~2.5 ppm, associated with Al(VI), while resonances observed at ~60 and 45 ppm were attributed to Al(IV). The intense signal at 45 ppm on the spectra for fly ash F3 was attributed to the tetrahedral aluminum in mullite, where three shares one oxygen atom surrounding Al tetrahedral (Sanz et al., 1988; Merwin et al., 1991). Ashes
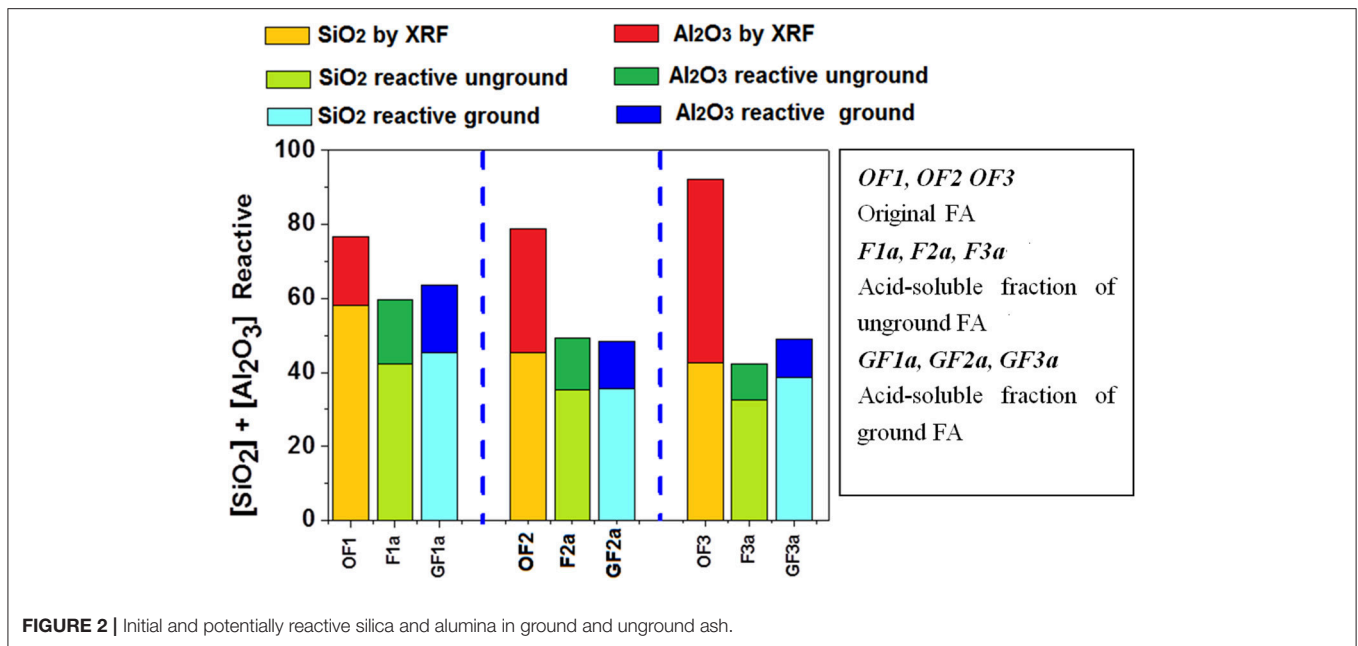
FIGURE 2 | Initial and potentially reactive silica and alumina in ground and unground ash.

F2 and F3 also exhibited a very intense signal at around 12 ppm, generated by the octahedral aluminum in corundum. This octahedral aluminum would explain the findings shown in **Figure 2**, according to which although the bulk aluminum content (∼33–50%) was high in these materials, less than half (14–15%) was dissolved by the acid. Hence the intensity of the Al$_O$ signals on the spectra for these two ashes.

The ^{27}Al spectra for F2 and F3 after grinding, also shown in **Figure 3** by way of example, were practically identical to those for the unground ash. The sole difference, the slightly lower post-grinding intensity of the shoulder at 2.5 ppm associated with mullite, may have been the result of the reduction in mullite crystal size, together with surface amorphisation of the mineral. In a study on the mechanical amorphisation of mullite drew similar conclusions (Schmucker et al., 1998). After grinding mullite for 240 h, they observed that the signal at 45 ppm was gradually replaced by one at 30 ppm, which appeared to grow at the expense of the resonances for both the tetrahedral and octahedral aluminum. In this study, whilst the intensity of the Al(VI) shoulder clearly declined, no signal was detected at 30 ppm. The apparent thrust of these findings was that mechanical activation did not significantly alter the coordination of the aluminum present in the ash: i.e., the tetrahedral and octahedral environments were the same in the ground and initial materials.

The ^{29}Si MAS-NMR spectra for the original ash (see **Figure 4**) exhibited a wide, poorly defined signal that actually enveloped a series of overlapping resonances. The area of the spectrum with absolute values greater than−108 ppm was attributed to the presence of crystal phases with Q^4(0Al) environments, such as quartz (-108 to−109 ppm) and cristobalite (-113 to−114 ppm) (Engelhardt and Michel, 1987). The area between−80 and−104 ppm was primarily identified with Q^4(mAl) units in the vitreous component of the ash (Criado et al., 2008). The signal at around−87 to−88 ppm, clearly visible on the F3, and

as a shoulder on the F2 spectrum, was attributed to the presence of a less polymerized (more reactive) glassy component. This area may also contain a signal attributed to the Q^3(3Al) units in crystalline mullite. The ash F1 spectrum exhibited a small peak at−71 ppm. Also observed but less clearly on the spectra for the other materials, that resonance may be due to the presence of scantly crystalline calcium silicate, which would partly explain the CaO content present in this ash (∼10%).

Figure 4 also reproduces ^{29}Si spectra for F2 and F3 after grinding (GF2 and GF3), by way of example. Analogously to the Al spectra, the Si spectra showed no significant variations in the Si atoms after mechanical activation. In short, milling fly ash had a substantial effect on fineness and its distribution, but a much lesser impact on its potentially reactive silica and alumina content. A slight variation in the aluminum environments was nonetheless observed, possibly due to surface amorphisation of minority crystalline particles such as mullite. This effect was more visible in the ashes with a higher percentage of such minority crystalline phases, namely F2 and F3, despite the rather shorter ("medium" intensity) grinding time than applied in other studies (Marjanovic et al., 2014).

Alkali Activation of Fly Ash

Table 2 gives the compressive strength of the pastes obtained by activating the unground and ground ashes with 8 M NaOH. All the ground ash pastes exhibited strength values at least 40–50% higher than their unground counterparts. The most striking difference was observed for ash F3. When mixed with 8 M NaOH, the unground ash hardened but was scantly compact and broke readily. Such an indication of poor quality might lead to the rejection of this ash. When the ash was ground, however, the resulting paste reached a strength of 18 MPa, a value comparable to those observed for the other materials before grinding. These findings attest to the significant role played by fineness in the

FIGURE 3 | ^{27}Al MAS-NMR spectra for ash **(A)** F1 **(B)** F2, and **(C)** F3.

FIGURE 4 | ^{29}Si MAS-NMR spectra for ash **(A)** F1 **(B)** F2, and **(C)** F3.

FIGURE 5 | Rate of Heat release for the different coal fly ashes activated with an 8 M NaOH solution at 85°C **(A)** F1Na (unground) and GF1Na (ground) **(B)** F2Na (unground) and GF2Na (ground) **(C)** F3Na (unground) and GF3Na (ground).
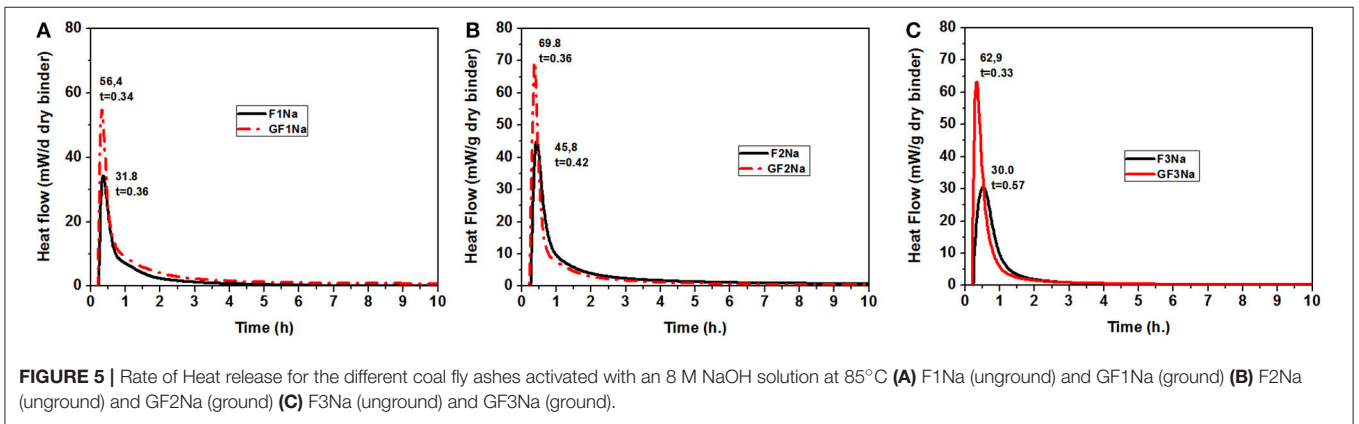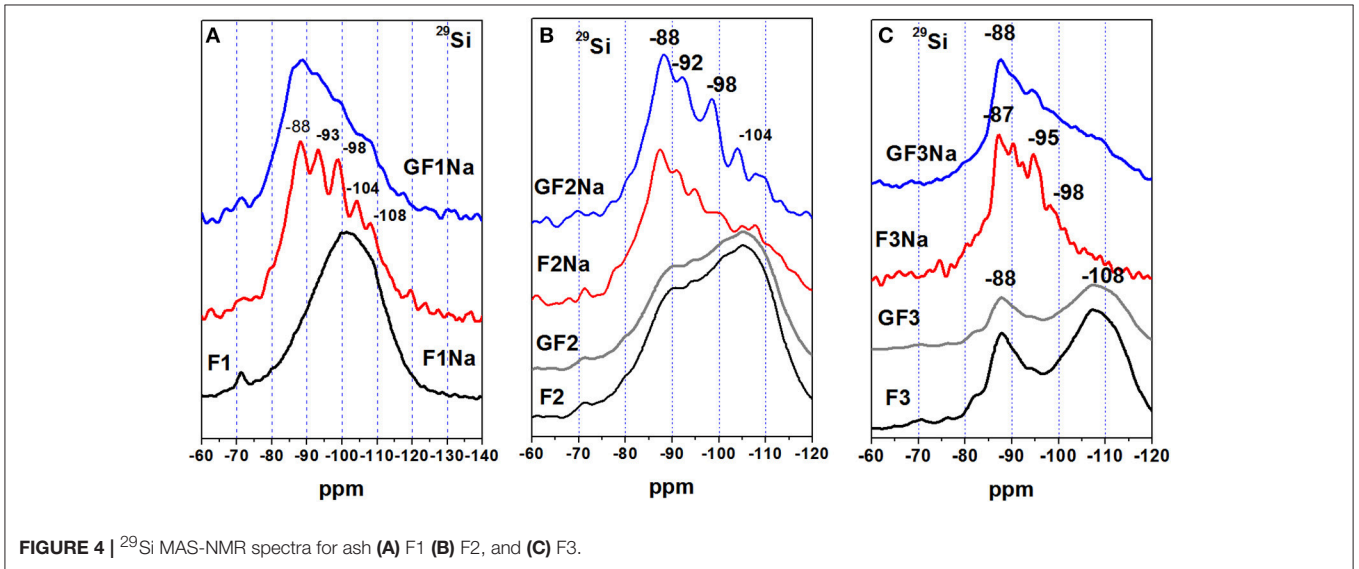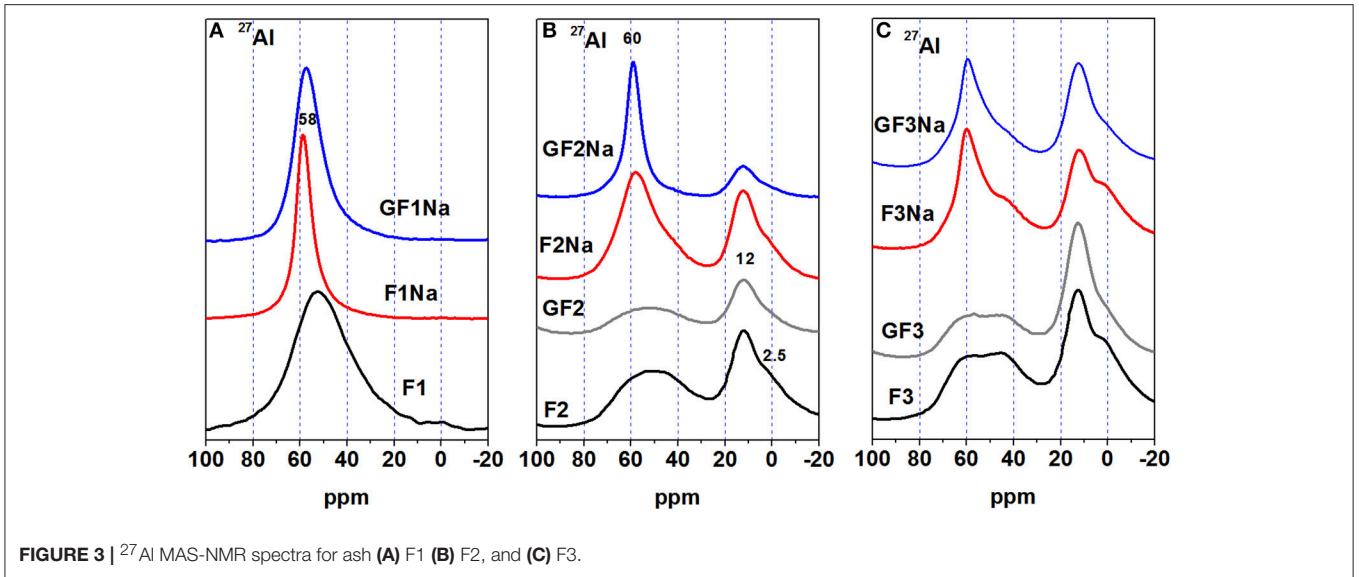
development of mechanical strength in cements made with alkali-activated fly ash.

Figure 5 shows the heat curves for the ground and unground fly ash pastes activated with an 8 M solution of NaOH at 85°C. Peak intensity was nearly double and appeared slightly earlier in all the pastes made with ground ash. The latter effect was more visible in ash F3, which initially had the coarsest particle size. These findings corroborated earlier reports (Zhang et al., 2016) to the effect that reducing the mean particle size raised the early age reaction rate in the material.

The XRD patterns for the initial fly ash and the activated pastes made with both ground and unground ash are reproduced in **Figure 6**. The most prominent features of the diffractograms were:

- the persistence of the same crystalline phases in the pastes as observed in the initial ash, confirming their low reactivity in alkaline media
- a shift in the hump of the pastes to slightly higher 2Θ values (25–40°), attesting to the formation of a N-A-S-H gel (Fernández-Jiménez et al., 2005)
- the presence of diffraction lines on the patterns for the initial (unground) activated fly ash (F1Na, N2Na, and F3Na) associated with the presence of herschelite, hydroxysodalite and zeolite Y (see **Figure 6**), in contrast to the diffractograms for the activated pastes prepared with ground ash (GF1Na, GF2Na, and GF3Na), on which no zeolite phases were detected.

The ^{27}Al and ^{29}Si MAS NMR spectra for the initial ash and ground and unground activated materials are reproduced in **Figures 3**, **4**. A comparison of these spectra revealed clear differences.

The signal at +58 to +60 ppm associated with Al(IV) (AlQ^4(4Si)-type units) present both in the N-A-S-H gel formed and in the zeolites was narrower and more intense on the ^{27}Al spectra (**Figure 3**) for the activated pastes made with ground and unground ash than on the spectra for the respective initial ashes. Pastes F1Na and GF1Na generated no signal that could be associated with Al(VI), for which no resonance was observed in the original ash either. The pastes prepared with ashes 2 and 3 (F2Na, GF2Na, F3Na, and GF3Na), in contrast, contained an intense signal at around 12 ppm, together with a shoulder at 2 ppm associated with the presence of Al(VI) in the crystalline phases of the initial ash (corundum and mullite). The signal for Al(IV) was narrower and more intense than the Al(VI) signal on the spectra for the pastes, whereas the opposite was observed on the spectra for the initial materials. The Al(VI) signal on the spectrum for paste GF2Na was very weak. Normally the Al$_O$ present in corundum and mullite is scantly responsive to alkaline activation. Here, however, ash grinding might be thought to have prompted a significant decline in corundum crystal size, along with surface amorphisation. As a result of the enhanced reactivity of this phase, part of the Al present would have subsequently been taken up in the matrix. That would explain the high strength values observed for the ground fly ash, despite its apparently low reactive Al content.
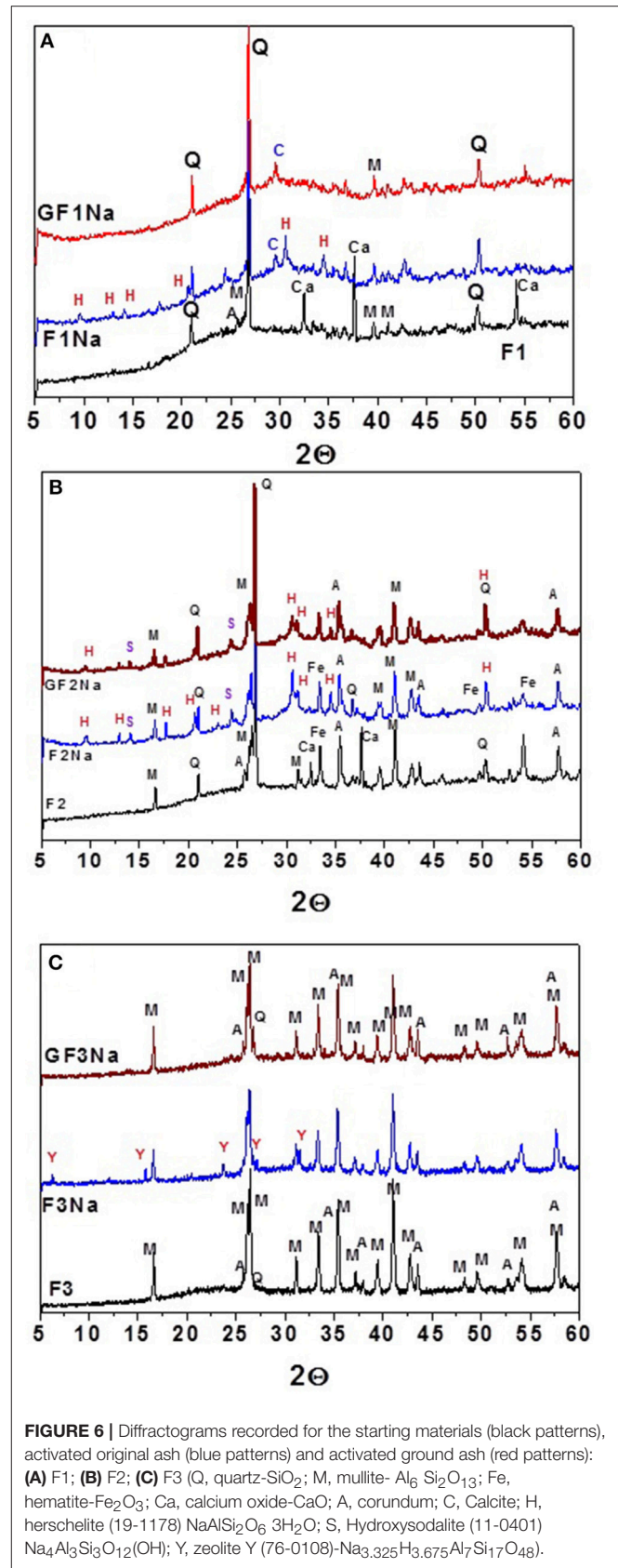
FIGURE 6 | Diffractograms recorded for the starting materials (black patterns), activated original ash (blue patterns) and activated ground ash (red patterns): **(A)** F1; **(B)** F2; **(C)** F3 (Q, quartz-SiO$_2$; M, mullite- Al$_6$Si$_2$O$_{13}$; Fe, hematite-Fe$_2$O$_3$; Ca, calcium oxide-CaO; A, corundum; C, Calcite; H, herschelite (19-1178) NaAlSi$_2$O$_6$ 3H$_2$O; S, Hydroxysodalite (11-0401) Na$_4$Al$_3$Si$_3$O$_{12}$(OH); Y, zeolite Y (76-0108)-Na$_{3.325}$H$_{3.675}$Al$_7$Si$_{17}$O$_{48}$).

The ^{29}Si spectra for the pastes also differed substantially from the spectra for the initial ashes (see **Figure 4**). Here the spectra for the unground ash pastes had more clearly defined signals, attributed to the higher zeolite content in these pastes, as observed in the XRD findings. As zeolites are more orderly structures than gels, their spectra are characterized by higher resolution. The ^{29}Si spectra for all the pastes exhibited a broad signal that masked overlapping resonances at positions at around $-88, -93, -98, -104,$ and -108 ppm, attributed to tetrahedral silicons, respectively, surrounded by Al_4, $SiAl_3$, Si_2Al_2, Si_3Al, and Si_4. The intensity of the signals varied with the ash (unground and ground). A signal detected at around -87 ppm, particularly intense in paste F3Na, was partly generated by the mullite present in the starting ashes (see spectra F3 and F3Na in **Figure 4C**).

The ^{23}Na spectra for the same pastes are reproduced in **Figure 7**. All contained a signal centered over -6.5 to -10 ppm, attributed to the presence of partially hydrated sodium, and needed to balance the charge in the geopolymer when silicon was replaced by aluminum in the aluminosilicate hydrate gel structure. As a rule, in aluminosilicate glass this signal shifts to more negative values when the Si/Al ratio rises and more positive values when it declines, very likely as the result of the increase in the Na-O interatomic distance or in the coordination numbers (Duxson et al., 2005; Provis et al., 2009). Paste F3Na, which exhibited the lowest strength, had two shoulders on its spectrum, one at around 3 ppm to 5 ppm associated with the Na in unbound $NaOH.nH_2O$ (Koller and Engelhardt, 1994) which is consistent with the lower degree of reaction in this paste, and the other at around -15 ppm, possibly attributable to sodium bonded with oxygen atoms only (Koller and Engelhardt, 1994; Duxson et al., 2005; Provis et al., 2009).

Figure 8 compares the microstructure of the chemically activated, ground and unground pastes made with ashes F1, F2, and F3. The pastes made with unground ash (F1Na, F2Na, and F3Na) were less compact on the whole than ground ash (GF1Na, GF2Na, and GF3Na) and contained a substantial number of unreacted glass microspheres, hollow (cenospheres) or filled with very small particles. The ground ash pastes (GF1Na, GF2Na, and GF3Na), especially GF3Na, had more compact matrices and a higher proportion of reacted ash. Zeolites were observed in the SEM micrographs of both ground and unground matrices, whereas XRD could detect them only in the pastes with unground ash. These data suggest that activation takes place so quickly in pastes with a high proportion of very fine particles that the new phases formed barely had time to develop a crystalline structure: i.e., reaction kinetics prevailed over thermodynamics.

Although qualitative, EDX analysis can approximate the compositional variability and homogeneity of the gels formed. The values in **Figure 9** are for $CaO-SiO_2-Al_2O_3$ and $Na_2O-SiO_2.Al_2O_3$ diagrams. Further to these data, very low calcium content ($\sim$2%) ash F3 formed which what was essentially a N-A-S-H gel. Ashes F1 and F2, with calcium contents of $\sim$10%, exhibited greater compositional variability. The matrices containing unground ash appeared to contain a heterogeneous mix of N,C-A-S-H-like gels with variable calcium contents (Garcia-Lodeiro et al., 2011; Walkley et al., 2016). A comparison
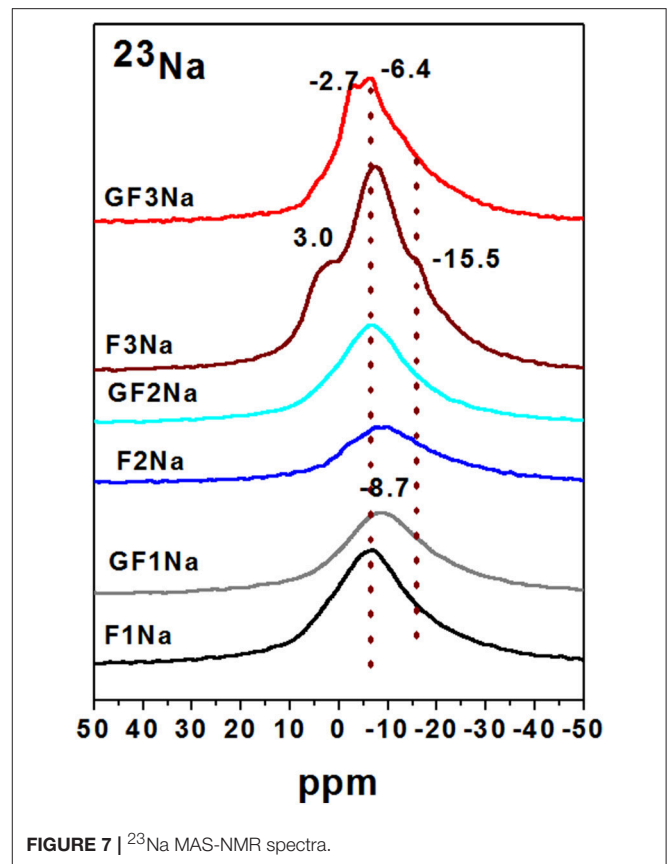
FIGURE 7 | ^{23}Na MAS-NMR spectra.

of the diagrams for F1 and F2 revealed that in the gels formed, the silicon/aluminum ratio was greater in the pastes prepared with ash F2, possibly due to the lower proportion of reactive aluminum present. When the ash was ground, the point distribution (red points) was slightly more homogeneous, indicating that mechanical activation, in addition to reducing the particle size, afforded the original ash a more uniform composition. As a result, the mean composition of the gels forming in pastes with ground ash was more homogeneous.

The findings for a given ash before and after grinding, compared here to determine the effect of fineness in materials with the same chemical composition, showed that the proportion of potentially reactive phase was only slightly modified by mechanical activation. Reaction kinetics and mechanical strength, however, rose significantly. These data are consistent with results reported by Zhang et al. (2016) suggesting that physical properties may play a more prominent role in ash reactivity than vitreous phase content or composition.

The smaller particle size in ground ash modified reaction kinetics, hastened dissolution and raised the initial degree of reaction, thereby generating higher early age strength. Smaller sized ash particles favored Al and Si dissolution in the medium as well as the precipitation of an N,C-A-S-H-like cementitious gel, which also affected material mineralogy and microstructure. The speedier reaction allowed practically no time for zeolites to crystallize or for the crystals to grow large enough to be detected by XRD. Another factor that may affect zeolite formation is the
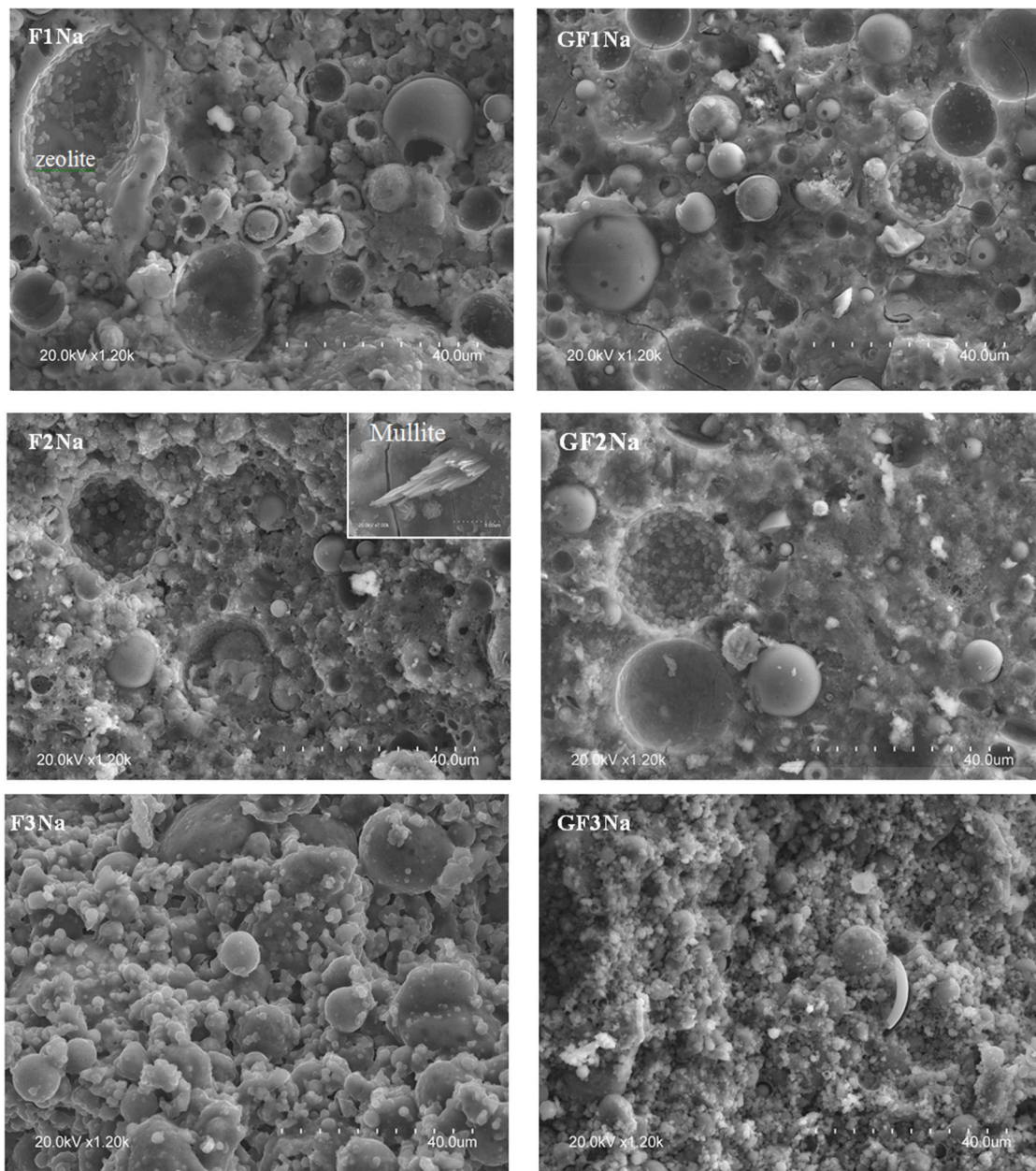
FIGURE 8 | SEM micrographs of pastes.

need for space. As **Figure 8** shows, zeolites form preferably inside cenospheres where they have sufficient space to crystallize and grow. Grinding the ash breaks these hollow particles, leaving a smaller number of voids. Fewer zeolites and more N-A-S-H gel raise mechanical strength (Panias et al., 2007; Criado et al., 2008).

Further to these data, for ash with similar vitreous phase contents, reducing the particle size substantially raises the mechanical strength that can be developed during alkaline activation. The question posed is: given a similar particle size, how does vitreous phase content affect ash reactivity? Although after grinding the three ashes had very similar particle size (d50

ranges between 5 and 7 μm), their mechanical strength values differed significantly. According to the proportion of potentially reactive phase identified by attacking the ash with acid (see **Figure 2**), the highest strength should have been recorded for ash GF1 followed by GF2 and GF3. Nonetheless, mechanical strength was the greatest in ash GF2.

Many studies have attempted to establish a criterion for assessing ash quality for the manufacture of alkaline cements (Fernández-Jiménez and Palomo, 2003; Fernández-Jiménez et al., 2005; Zhuang et al., 2016). The present authors deem that vitreous phase content, $(SiO_2/Al_2O_3)_{reactive}$ ratio and fineness are
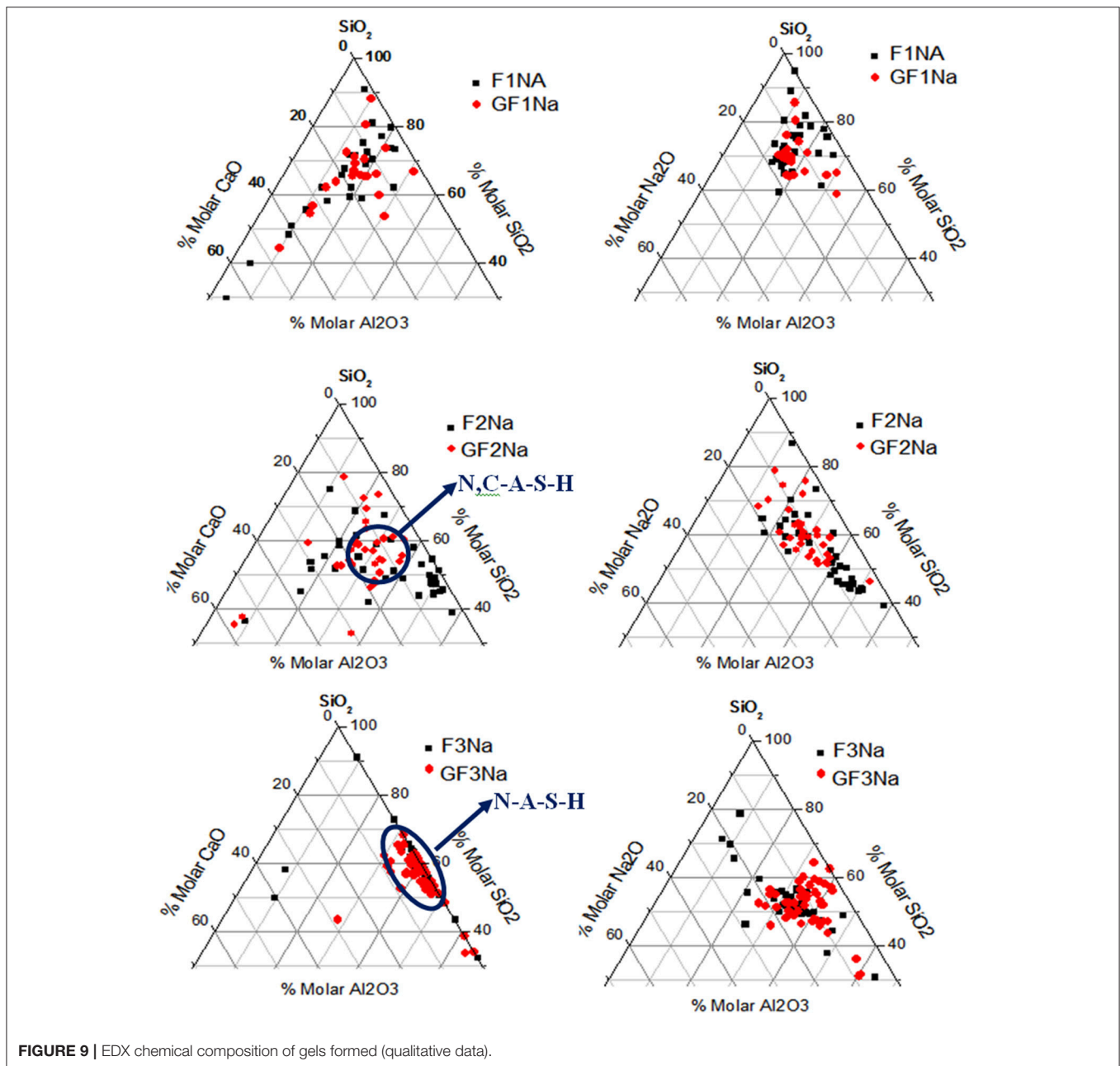
FIGURE 9 | EDX chemical composition of gels formed (qualitative data).

determinants that provide an approximate idea of the reactive potential of an ash. Nonetheless, the findings reported here suggest the existence of yet another parameter that may affect ash reactivity. The effect of minority elements in the ash (network modifiers such as alkalis, calcium, titanium, or iron) must be taken into consideration, inasmuch as their inclusion in the glass structure may modify its solubility. Presumably, the higher the concentration of such elements in the vitreous phase, the greater its glass reactivity. That hypothesis concurs partially with the one put forward by Zhang et al. (2016).

Determining the presence of network modifiers in the vitreous phase with the techniques deployed here is hardly

straightforward. Comparing the ^{29}Si NMR spectra for ashes F1 and F2, however, revealed that the zone between -80 and -100 ppm was more intense in the latter than in the former. That may be indicative of a less polymerized and consequently more reactive glass, which would explain the higher strength in F2, fruit of a higher initial degree of reaction. The present authors feel, however, that the structure and composition of the gel forming as the main reaction product is another factor to be borne in mind when explaining mechanical strength. The EDX findings (see **Figure 9**) showed that as a rule the gel forming in pastes F2Na and GF2Na had a higher SiO_2/Al_2O_3 ratio, a finding consistent with the higher $(SiO_2/Al_2O_3)_{reactive}$ ratio determined

by acid attack. Reports can be found in the literature showing that more silica-rich N-A-S-H gels yield higher strength alkaline cements (Fernández-Jiménez et al., 2006; Criado et al., 2008; Provis et al., 2009).

The suitability of coal fly ash for manufacturing alkaline cements can in any event be predicted fairly precisely on the grounds of physical, mineralogical and chemical parameters (fineness, chemical composition, vitreous phase content...), which can approximate reactivity. Nonetheless, given a vitreous phase content that can be regarded as acceptable (>30%, see ash F3), fineness prevails over glass content.

This fact is promising with a view to raising fly ash reactivity. The mineralogical and chemical compositions of ash depend essentially on the coal and burning conditions used in steam-fired power plants and are consequently very difficult to control or modify. Fineness, in contrast, can be readily established and manipulated. This study shows that in ash with <80–90% of particles under $45\,\mu m$, grinding would suffice to raise reactivity substantially. Ash such as F3 that initially failed to harden into a sufficiently compact specimen when alkali-activated, after grinding yielded mechanical strength of up to 18 MPa, a value similar to that was observed for unground ash F1.

CONCLUSIONS

The conclusions drawn from the findings of this study are listed below:

- Fly ash reactivity depends essentially on fineness, vitreous phase content and chemical composition ($(SiO_2/Al_2O_3)_{reactive}$). Modifying the first parameter via mechanical activation is unquestionably the simplest way to heighten and control reactivity.
- Mechanical activation has only a minor effect on fly ash reactivity, inasmuch as the amount of potentially reactive SiO_2 and Al_2O_3 depends more on the mineralogical phases in the ash than on fineness.

- The mechanical activation of fly ash enhanced initial strength development substantially in the alkaline cements studied due to reaction kinetics: more ash reacted in less time.
- Mechanical activation of ash affects the nature of the reaction products formed: a faster reaction rate generates more N-A-S-H or N,C-A-S-H gel and fewer zeolites as secondary reaction products. A higher gel content contributes to higher mechanical strength.
- In this study, which compared ashes with different chemical compositions, mechanical activation of the materials was observed to enhance mechanical strength development substantially, partially offsetting low vitreous phase contents or scantly optimal $(SiO_2/Al_2O_3)_{reactive}$ ratios.

AUTHOR CONTRIBUTIONS

IG-L and OM conducted the experiments, data analyses and characterizations. AF-J and IG-L drafted the manuscript. AP helped with manuscript preparation and supervised the overall research. AF-J and IG-L finalized the manuscript.

ACKNOWLEDGMENTS

SUPPLEMENTARY MATERIAL

The Supplementary Material for this article can be found online at: https://www.frontiersin.org/articles/10.3389/fmats.2019.00051/full#supplementary-material

Figure S1 | SEM Micrographs of the coal fly ashes before (F1, F2 and F3) and after grinding (F1G, F2G and F3G).

REFERENCES

Bai, C., and Colombo, P. (2018). Processing, properties and applications of highly porous geopolymers: a review. *Ceramics Int.* 44, 16103–16118. doi: 10.1016/j.ceramint.2018.05.219

Chindaprasirt, P., De Silva, P., Sagoe-Crentsil, K., and Hanjitsuwan, S. (2012). Effect of SiO_2 and Al_2O_3 on the setting and hardening of high calcium fly ash-based geopolymer systems. *J. Mater. Sci.* 47, 4876–4883. doi: 10.1007/s10853-012-6353-y

Chindaprasirt, P., Jaturapitakkul, C., and Sinsiri, T. (2005). Effect of fly ash fineness on compressive strength and pore size of blended cement paste. *Cem. Concr. Compos.* 27, 425–432. doi: 10.1016/j.cemconcomp.2004.07.003

Communication from the Commission to the European Parliament, the Council, the European Economic and Social Committee and the Committee of the Regions (2011). *Roadmap to a Resource Efficient Europe* (COM), 571. Available online at: http://eur-lex.europa.eu/legal-content/EN/TXT/?uri=CELEX:52011DC0571

Criado, M., Fernández-Jiménez, A., Palomo, A., Sobrados, I., and Sanz, J. (2008). Effect of the SiO_2/Na_2O ratio on the alkali activation of fly ash. Part II: ^{29}Si MAS-NMR Survey. *Micropor. Mesopor. Mater.* 109, 525–534. doi: 10.1016/j.micromeso.2007.05.062

CSI/ECRA—Cement Sustainability Initiative/ European Cement Research. (2017). *Technology Papers 2017 Development of State of the Art Techniques in Cement Manufacturing: Trying to Look Ahead, Dusseldorf, Geneva.* Available online at: www.wbcsdcement.org (Accessed December 30, 2017).

De Silva, P., Sagoe-Crenstil, K., and Sirivivatnanon, V. (2007). Kinetics of geopolymerization: role of Al_2O_3 and SiO_2. *Cem. Concr. Res.* 37, 512–518. doi: 10.1016/j.cemconres.2007.01.003

Duvallet, T., Frouin, L., and Robl, L. T. (2015). "Effect of fly ash particle packing on performance of OPC-activated GGBS slag," *Presented at the 2015 World of Coal Ash Conference* (Nashville).

Duxson, P., Lukey, G. C., Separovic, F., and van Deventer, J. S. J. (2005). Effect of alkali cations on aluminum incorporation in geopolymeric gels. *Ind. Eng. Chem. Res.* 44, 832–839. doi: 10.1021/ie0494216

Engelhardt, G., and Michel, D. (1987). *High Resolution Solid State NMR of Silicates and Zeolites*. New York, NY: John Wiley and Sons.

Fernández-Jiménez, A., Cristelo, N., Miranda, T., and Palomo, A. (2017). Sustainable alkali activated materials: precursor and activator derived from industrial wastes. *J. Cleaner Prod.* 162, 1200–1209. doi: 10.1016/j.jclepro.2017.06.151

Fernández-Jiménez, A., and Palomo, A. (2003). Characterization of fly ashes. Potential reactivity as alkaline cements. *Fuel* 82, 2259–2265. doi: 10.1016/S0016-2361(03)00194-7

Fernández-Jiménez, A., and Palomo, A. (2007). Factors affecting early compressive strength of alkali activated flys ash (OPC fee) concrete. *Mater. Construct.* 57, 7–22.

Fernández-Jiménez, A., Palomo, A., and Criado, M. (2005). Microstructure development of alkali-activated fly ash cement: a descriptive model. *Cem. Concr. Res.* 35, 1204–1209. doi: 10.1016/j.cemconres.2004.08.021

Fernández-Jiménez, A., Palomo, A., Sobrados, I., and Sanz, J. (2006). The role played by the reactive alumina content in the alkaline activation of fly ashes. *Microporous Mesoporous Mater.* 91, 111–119. doi: 10.1016/j.micromeso.2005.11.015

Garcia-Lodeiro, I., Fernández-Jiménez, A., and Palomo, A. (2013). Variation in hybrid cements over time. Alkaline activation of fly ash–portland cement blends. *Cem. Concr. Res.* 52, 112–122. doi: 10.1016/j.cemconres.2013.03.022

Garcia-Lodeiro, I., Palomo, A., Fernández-Jiménez, A., and Macphee, D. E. (2011). Compatibility studies between N-A-S-H and C-A-S-H gels. Study in the ternary diagram Na_2O–CaO–Al_2O_3–SiO_2-H_2O. *Cem. Concr. Res.* 41, 923–931. doi: 10.1016/j.cemconres.2011.05.006

Hajimohammadi, A., Provis, J. L., and van Deventer, J. S. J. (2010). Effect of alumina release rate on the mechanism of geopolymer gel formation. *Chem. Mater.* 22, 5199–5208. doi: 10.1021/cm101151n

Hemalatha, T., and Ramaswamy, A. (2017). A review on fly ash characteristics e towards promoting high volume utilization in developing sustainable concrete. *J. Cleaner Prod.* 147, 546–559. doi: 10.1016/j.jclepro.2017.01.114

Koller, H., and Engelhardt, G. (1994). ^{23}Na NMR spectroscopy of solids: interpretation of quadrupole. Interaction parameters and chemical shifts. *J. Phys. Chem.* 98, 1544–1551. doi: 10.1021/j100057a004

Kovalchuk, G., Fernández-Jiménez, A., and Palomo, A. (2007). Alkali-activated fly ash: effect of thermal curing conditions on mechanical and microstructural development—Part II. *Fuel* 86, 315–322. doi: 10.1016/j.fuel.2006.07.010

Kumar, S., Kristály, F., and Mucsi, G. (2015). Geopolymerisation behaviour of size fractioned fly ash. *Adv. Powder Technol.* 26, 24–30. doi: 10.1016/j.apt.2014.09.001

Kumar, S., and Kumar, R. (2011). Mechanical activation of fly ash: effect on reaction, structure and properties of resulting geopolymer. *Ceram. Inter.* 37, 533–541. doi: 10.1016/j.ceramint.2010.09.038

Marjanovic, N., Komljenovic, M., Baščarevic, Z., and Nikolic, V. (2014). Improving reactivity of fly ash and properties of ensuing geopolymers through mechanical activation. *Constr. Build. Mater.* 57, 151–162. doi: 10.1016/j.conbuildmat.2014.01.095

Merwin, L. H., Sebald, A., Rager, H., and Schneider, H. (1991). ^{29}Si and ^{27}Al MAS NMR spectroscopy of mullite. *Phys. Chem. Minerals* 18, 47–52. doi: 10.1007/BF00199043

Nikolic, V., Komljenovic, M., Baščarevic, Z., Marjanovic, N., Miladinovic, Z., and Petrovic, R. (2015). The influence of fly ash characteristics and reaction conditions on strength and structure of geopolymers. *Construct. Build. Mater.* 94, 361–370. doi: 10.1016/j.conbuildmat.2015.07.014

Palomo, A., Krivenko, P., Garcia-Lodeiro, I., Kavalerova, E., Maltseva, O., and Fernández-Jiménez, A. (2014). A review on alkaline activation : new analytical perspectives. *Mater. Construct.* 641, 23. doi: 10.3989/mc.2014.00314

Panias, D., Giannopoulou, I. P., and Perraki, T. (2007). Effect of synthesis parameters on the mechanical properties of fly ash-based geopolymers. *Colloids Surf A* 301, 246–54. doi: 10.1016/j.colsurfa.2006.12.064

Paya, J., Monzo, J., Borrachero, M. V., Peris, E., and Gonzalez-Lopez, E. (1997). Mechanical treatment of fly ashes. Part III: studies on strength development of ground fly ashes (GFA) – cement mortars. *Cem. Concr. Res.* 27, 1365–77. doi: 10.1016/S0008-8846(97)00129-4

Provis, J., and van Deventer, J. S. J. (2014). *Alkali Activated Materials: State-of-the-Art Report*. London, UK: Springer.

Provis, J. L., Yong, C. Z., Duxon, P., and van Deventer, J. S. J. (2009). Correlating mechanical and thermal properties of sodium silicate-fly ash geopolymer. *Colloids Surf. A Physicochem. Eng. Asp.* 336, 57–63. doi: 10.1016/j.colsurfa.2008.11.019

Rakesh, K., Sanjay, K., and Mehrotra, S. P. (2007). Towards sustainable solutions for fly ash through mechanical activation Resources. *Resour. Conserv. Recycl.* 52, 157–179. doi: 10.1016/j.resconrec.2007.06.007

Ruiz-Santaquiteria, C., Skibsted, J., Fernández-Jiménez, A., and Palomo, A. (2013). Clay reactivity: production of alkali activated cements. *Appl. Clay Sci.* 73, 11–16. doi: 10.1016/j.clay.2012.10.012

Sagoe-Crentsil, L. W., Brown, T., and Song, S. (2005). Effects of aluminates on the formation of geopolymers. *Mater. Sci. Eng. B* 117, 163–168. doi: 10.1016/j.mseb.2004.11.008

Sanz, J., Madani, A., Serratosa, J. M., Moya, J. S., and Aza, S. (1988). Aluminum-27 and Silicon-29 Magic-Angle Spinning Nuclear Magnetic Resonance Study of the Kaolinite-Mullite Transformation. *J. Amer. Cer. Soc.* 71, 3024–3028. doi: 10.1111/j.1151-2916.1988.tb07513.x

Schmucker, M., Schneider, H., and MacKenzie, K. J. D. (1998). Mechanical amorphization of mullite and thermal recrystallization. *J. Non-Crystalline Sol.* 226, 99–104. doi: 10.1016/S0022-3093(98)00366-4

Shekhovtsova, J., Zhernovsky, I., Kovtun, M., Kozhukhova, N., Zhernovskaya, I., and Kearsley, E. (2018). Estimation of fly ash reactivity for use in alkali activated cements step towards sustainable building material and waste utilization. *J. Cleaner Prod.* 178, 22–33. doi: 10.1016/j.jclepro.2017.12.270

Temuujin, J., Williams, R. P., and van Riessen, A. (2009). Effect of mechanical activation of fly ash on the properties of geopolymer cured at ambient temperature. *J. Mater. Process. Technol.* 209, 5276–5280. doi: 10.1016/j.jmatprotec.2009.03.016

Thomas, M. (2007). *Optimizing the Use of Fly Ash in Concrete Association*. Available online at: http://www.cement.org/docs/default-source/fc_concrete_technology/is548-optimizing-the-use-of-fly-ash-concrete.pdf (Accessed April 2, 2017).

Walkley, B., San Nicolas, R., Sani, M. A., Rees, G. J., Hanna, J. V., van Deventer, J. S. J., et al., (2016). Phase evolution of C-(N)-A-S-H/N-A-S-H gel blends investigated via alkali-activation of synthetic calcium aluminosilicate precursors. *Cem. Concr. Res.* 89, 120–135. doi: 10.1016/j.cemconres.2016.08.010

Zhang, Z., Provis, J. L., Zou, J., Reide, A., and Wang, H. (2016). Towards an indexing approach to evaluate fly ashes for geopolymer manufacture. *Cem. Concr. Res.* 85, 163–173. doi: 10.1016/j.cemconres.2016.04.007

Zhou, W., Yan, C., Duan, P., Liu, Y., Zhang, Z., Qiu, X., et al., (2016). A comparative study of high- and low-Al_2O_3 fly ash based-geopolymers: the role of mix proportion factors and curing temperature. *Mater. Des.* 95 63–74. doi: 10.1016/j.matdes.2016.01.084

Zhuang, X. Y., Chen, L., Komarneni, S., Zhou, C. H., Tong, D. S., Yang, H. M., et al., (2016). Fly ash-based geopolymer: clean production, properties and applications. *J. Cleaner Prod.* 125, 253–267. doi: 10.1016/j.jclepro.2016.03.019